Click Addition of a DNA Thread to the N-Termini of Peptides for Their Translocation through Solid-State Nanopores

Sudipta Biswas,[†,‡,⊥] Weisi Song,[†,§,⊥] Chad Borges,[†,‡] Stuart Lindsay,[*,†,‡,§] and Peiming Zhang[*,‡]

[†]Biodesign Institute, [‡]Department of Chemistry and Biochemistry, [§]Department of Physics, Arizona State University, Tempe, Arizona 85287, United States. [⊥]SB and WS contributed equally.

ABSTRACT Foremost among the challenges facing single molecule sequencing of proteins by nanopores is the lack of a universal method for driving proteins or peptides into nanopores. In contrast to nucleic acids, the backbones of which are uniformly negatively charged nucleotides, proteins carry positive, negative and neutral side chains that are randomly distributed. Recombinant proteins carrying a negatively charged oligonucleotide or polypeptide at the C-termini can be translocated through a α-hemolysin (α-HL) nanopore, but the required genetic engineering limits the generality of these approaches. In this present study, we have developed a chemical approach for addition of a charged oligomer to peptides so that they can be translocated through nanopores. As an example, an oligonucleotide PolyT$_{20}$ was tethered to peptides through first selectively functionalizing their N-termini with azide followed by a click reaction. The data show that the peptide-PolyT$_{20}$ conjugates translocated through nanopores, whereas the unmodified peptides did not. Surprisingly, the conjugates with their peptides tethered at the 5′-end of PolyT$_{20}$ passed the nanopores more rapidly than the PolyT$_{20}$ alone. The PolyT$_{20}$ also yielded a wider distribution of blockade currents. The same broad distribution was found for a conjugate with its peptide tethered at the 3′-end of PolyT$_{20}$, suggesting that the larger blockades (and longer translocation times) are associated with events in which the 5′-end of the PolyT$_{20}$ enters the pore first.

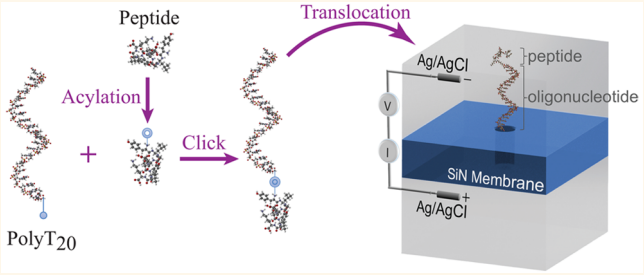

KEYWORDS: nanopore · protein sequencing · DNA thread · click addition · peptide-PolyT$_{20}$ conjugate · peptide translocation

Nanopores—orifices with nanometer diameters—can function as nanofluidic channels for the flow of ions and the transport of biomolecules. When a charged molecule is electrophoretically driven through the nanopore, it partially obstructs the passage of ions and modulates the current through the pore. Parameters derived from the current blockade can be used to identify the molecule and even identify structural subunits. Nanopore techniques are emerging as a single molecule tool for sequencing DNA,[1] detecting proteins,[2] polysaccharides,[3] and viruses,[4] with possible clinical applications.[5] As protein-based nanopore DNA sequencing technology makes inroads into genomic research,[6−8] the question arises: can nanopores sequence proteins as well? Given the fact that even a MspA protein nanopore (which has a finer nanopore—0.5 nm thickness and 1.2 nm diameter—than α-hemolysin) only demonstrates a four-nucleotide resolution[1] with ∼85% accuracy,[9] it seems unlikely that ion-current blockade measurements will ever resolve individual amino acids because calling each of the amino acids requires sorting 20[4] or 160 000 different signals. A new reading mechanism has to be developed to achieve single amino acid residue resolution for protein sequencing. Electron tunneling detection has been shown to have this capability. Recently, we have demonstrated that individual amino acids can be identified and two different peptides distinguished at a single molecule level by a technique we call recognition tunneling, which measures tunneling currents of analytes in a ∼2.5 nm nanogap with its two electrodes functionalized with

* Address correspondence to peiming.zhang@asu.edu, stuart.lindsay@asu.edu.

Received for review January 28, 2015 and accepted September 12, 2015.

Published online September 12, 2015
10.1021/acsnano.5b04984

recognition molecules.[10] Kawai and co-workers have also reported the identification of amino acids and phosphorylated peptides by means of electron tunneling currents with either 0.5 or 0.7 nm nanogaps.[11] Thus, one can conceive of a device that integrates a tunneling gap with a solid-state nanopore for analyzing protein sequences.

Here, we address another key roadblock to developing nanopore technology for proteomics, which is the translocation of proteins and peptides. While DNA is uniformly negatively charged along its phosphate backbone under physiological conditions, a protein can carry zero, positive or negative net charge, the sum of the charges of the positively and negatively charged side chains that are randomly distributed on its amide backbone. This makes electrophoretic translocation of the protein challenging. Furthermore, owing to the lack of a PCR-like technique for amplifying proteins, it is very difficult to even acquire direct evidence to prove protein translocation.[12] Recently, Akeson and his co-workers demonstrated that a recombinant ubiquitin-like protein Smt3 bearing a polyanionic peptide at its C-terminus was unfolded and pulled through a α-hemolysin (α-HL) nanopore by the AAA+ unfoldase ClpX.[13] Almost at the same time, Bayley's team reported that a thioredoxin protein tethered to a negatively charged oligonucleotide could also be unfolded and translocated through the α-HL nanopore by an applied voltage.[14] These studies suggest a new approach to translocating proteins using a charged "pulling-string" to draw the protein into a nanopore.

With the ultimate goal of sequencing proteins, our initial objective has focused on using a recognition tunneling nanopore to identify peptides. As a matter of fact, the most commonly used method in proteomics is the shotgun mass spectrometry, in which proteins are first digested into peptides with enzymes (such as trypsin) that generate peptides containing only one lysine or arginine residue at their C-terminus. These are separated with liquid chromatography, and injected as charged ions into a mass spectrometer for identification.[15] It can also be a method to quantify proteins, for example, when applying a selected reaction monitoring (SRM) technique that uses a set of representative peptides as a surrogate for a protein.[16] We are adapting the SRM approach to our platform for analysis of proteins. While working on fabricating a fixed-gap tunnel junction in solid-state nanopores,[17] we have developed a molecular threading strategy to facilitate translocation of peptides: tethering a chain molecule with a large net charge, which functions as a molecular thread, to the termini of peptides to make them all have the same sign of charge so that they can be carried over from one side to another of a nanopore by the threading molecule under a voltage bias. Thus, a basic requirement for the threading molecule is that it can readily translocate through nanopores. We chose an oligonucleotide composed of 20 thymidine nucleotides (referred to as $PolyT_{20}$) as a negatively charged thread because the short oligonucleotide has well-defined structure and charge distribution, its translocation has been well studied,[18−20] and it is also readily available from commercial sources. In this present study, we have focused on developing a simple and effective chemistry for attaching the oligonucleotide to the N-termini of peptides, and have demonstrated the translocation of the DNA-peptide conjugates through solid-state nanopores.

RESULTS AND DISCUSSION

Addition of $PolyT_{20}$ to N-Termini of Peptides. We chose to functionalize the N-terminal α-amine of peptides because it is more nucleophilic than the C-terminal carboxylate, and so susceptible to chemical modification with electrophilic reagents in physiological conditions. The challenge is to find a reagent and conditions that selectively functionalize the α-amine in the presence of other nucleophiles, such as ε-amine of lysine. Although a plethora of chemical methods for modification of proteins have been reported in literature,[21] there is still lack of a universal chemistry to specifically modify the N-termini of peptides. In general, the selectivity and efficiencies of an N-terminal reaction vary with peptide sequences[22] and the amino acid residues at the end.[23,24] For example, in a very recent publication, MacDonald *et al.* have reported that 2-pyridinecarboxaldehyde (PCA) reacted with α-amine of peptide X-ADSWAG (X = one of 20 naturally occurring amino acids) with selectivity of varying from >50% to ~100%, averaging <90%.[25] In this present study, we describe the development of a general method for functionalization of the N termini of tryptic peptides with high selectivity. Acylation is a commonly used chemical reaction in the modification of proteins with chemical reagents such as carboxylic halide, carboxylic anhydride, or active ester.[21] We chose the carboxylic anhydride—which has been reported to selectively react with the N-terminal amines of peptides under neutral or slightly basic conditions[26,27]—to introduce a bioorthogonal function to N-termini of peptides for DNA attachment. As shown in Scheme 1, an azidoacetic anhydride reagent (see Methods for its synthesis) first reacts with a peptide bearing a lysine residue at its C-terminus, generating an *N*-azidoacetylated peptide under slightly acidic conditions (Step 1). This is followed by reaction of the azide group with aza-dibenzocyclooctyne (ADIBO) functionalized $PolyT_{20}$ through a click reaction, resulting in the desired DNA-peptide conjugate (Step 2). The ADIBO function—a strained cycloalkyne—specifically reacts with azide at a high reaction rate ($k = 0.3\ M^{-1}\ s^{-1}$) without need of a copper catalyst[28] (so-called copper free click chemistry[29]). Because of its bioorthogonality, the ADIBO-azide click

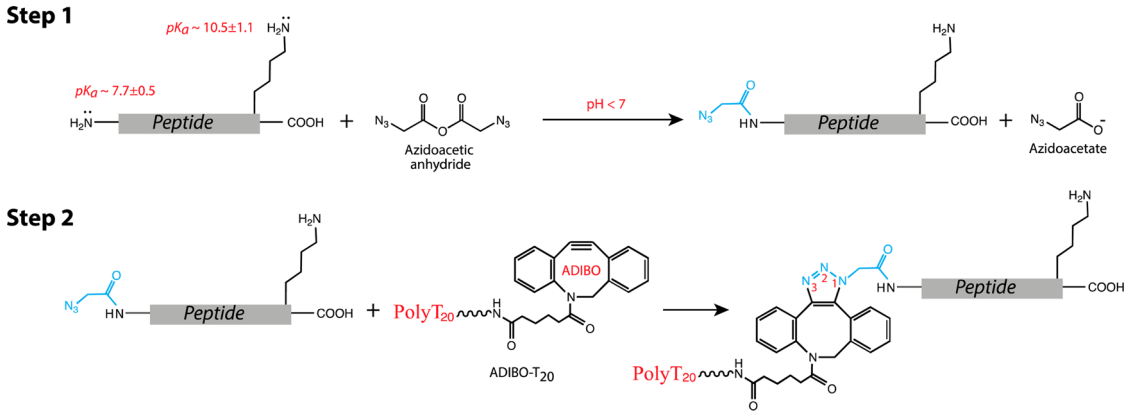

Scheme 1. Chemical reactions for attaching an oligonucleotide to N-termini of peptides.

TABLE 1. Peptide Sequences Used in This Study and Their Physicochemical Properties

	sequence	mass[a]	isoelectric point (pI)[a]	net charge at pH 7[a]	hydropathy index (h)[b]	diffusion coefficient (cm^2 s^{-})[c]	size[d] (*L*/*W*, nm)
P-1	YLGEEYVK	999.49	4.26	−1	−5.9	4.37×10^{-6}	2.3/1.0
P-2	DRVYIHPFHL	1295.68	7.91	+0.2	−2.0	3.89×10^{-6}	3.0/1.0
P-3	EAIYAAPFAKKK	1335.76	10.05	+2	−3.6	3.80×10^{-6}	3.8/1.0

[a] Calculated using the peptide property calculator in http://www.innovagen.com/custom-peptide-synthesis/peptide-property-calculator/peptide-property-calculator.asp. [b] Calculated by adding the hydropathy value for each amino acid residue together.[55] [c] Calculated based on equation log $D = -0.434 \log MW - 4.059$.[56] [d] Measured from the structure model calculated by molecular mechanics with Merck molecular force field (MMFF) in Spartan'14 (L = length; W = width).

reaction has been applied to forming conjugates of DNA with protein,[30] protein with protein,[31] protein with drugs,[32] to functionalizing gold nanoparticles,[33] to labeling aptamers[34] and RNA[35] with fluorescent dyes, to immobilizing proteins (or antibodies),[36−38] and peptides,[39] and to targeting tumor cells.[40] Given these advances in click chemistry, we paid more attention to the reaction of azidoacetic anhydride with peptides to optimize its selectivity. Besides the N-terminal α-amine, the acyl anhydride can react with the ε-amine of lysine, phenolate ion of tyrosine, sulfhydryl group of cysteine, aliphatic hydroxyl of serine and threonine, and the imidazolyl ring of histidine as well.[41] However, the intrinsic reactivity of these groups to an electrophile and stability of their acyl derivatives are all different. In most cases, the reactive groups involved in the acylation are the α- and ε-amine, imidazolyl ring, and to a lesser extent, −SH and −OH. The thioester and ester from acylation of cysteine, tyrosine, serine and threonine residues can be reversed to the original groups.[42] In an aqueous solution, these functional groups have distinguishable acid dissociation constants (pK_a): For example, an average pK_a value for ε-amine of lysine in proteins is 10.5, and for α-amine of the N-terminus it is 7.7.[43] Because a protonated amine is not reactive, this difference in pK_a creates room for us to tune the selectivity of the acylation reaction by changing the pH and, in turn, the protonation states of these amines (Step 1 in Scheme 1). We assumed that the slightly acidic conditions should achieve higher selectivity to the α-amine than the basic conditions.

We have studied three representative short peptides for the reactions shown in Scheme 1. The sequences and calculated physicochemical properties of these peptides (designated as **P-1**, **P-2**, and **P-3**, respectively) are listed in Table 1. In particular, **P-1** and **P-3** contain different numbers of lysines (K) and no histidine (H), and **P-2** has two histidines and no lysine. Each of them carries different net charge at neutral pH. These peptides have a similar width, ~1 nm at their widest. In addition, they are hydrophilic and have similar diffusion coefficients. Circular Dichroism (CD) showed that they took a random conformation in aqueous solution, whereas $PolyT_{20}$ adopted an organized right-handed helical conformation (Figure S1, Supporting Information) so that it may provide an entropic advantage for threading into a nanopore.

We began with **P-1**, a peptide that mimics a trypsin digest. First, we compared the selectivity of the anhydride with another commonly used acylating reagent *N*-hydroxysuccinimidyl (NHS) ester. The NHS azidoacetate reacted with **P-1** at pH 6.7, but produced two products that were characterized as a peptide modified by one and two azidoacetyl (N_3CH_2CO-) groups by MALDI mass spectrometry. In general, the NHS ester may preferentially react with the lysine amine. However, Mentinova *et al.* have showed that sulfo-NHS-acetate reacts preferentially with the N-terminal α-amine only at pH ~ 5, but did not report the reaction yield.[44] These facts further motivated us to use azidoacetic anhydride as an acylating reagent. Initially, the acylation reaction was carried out with **P-1** at a

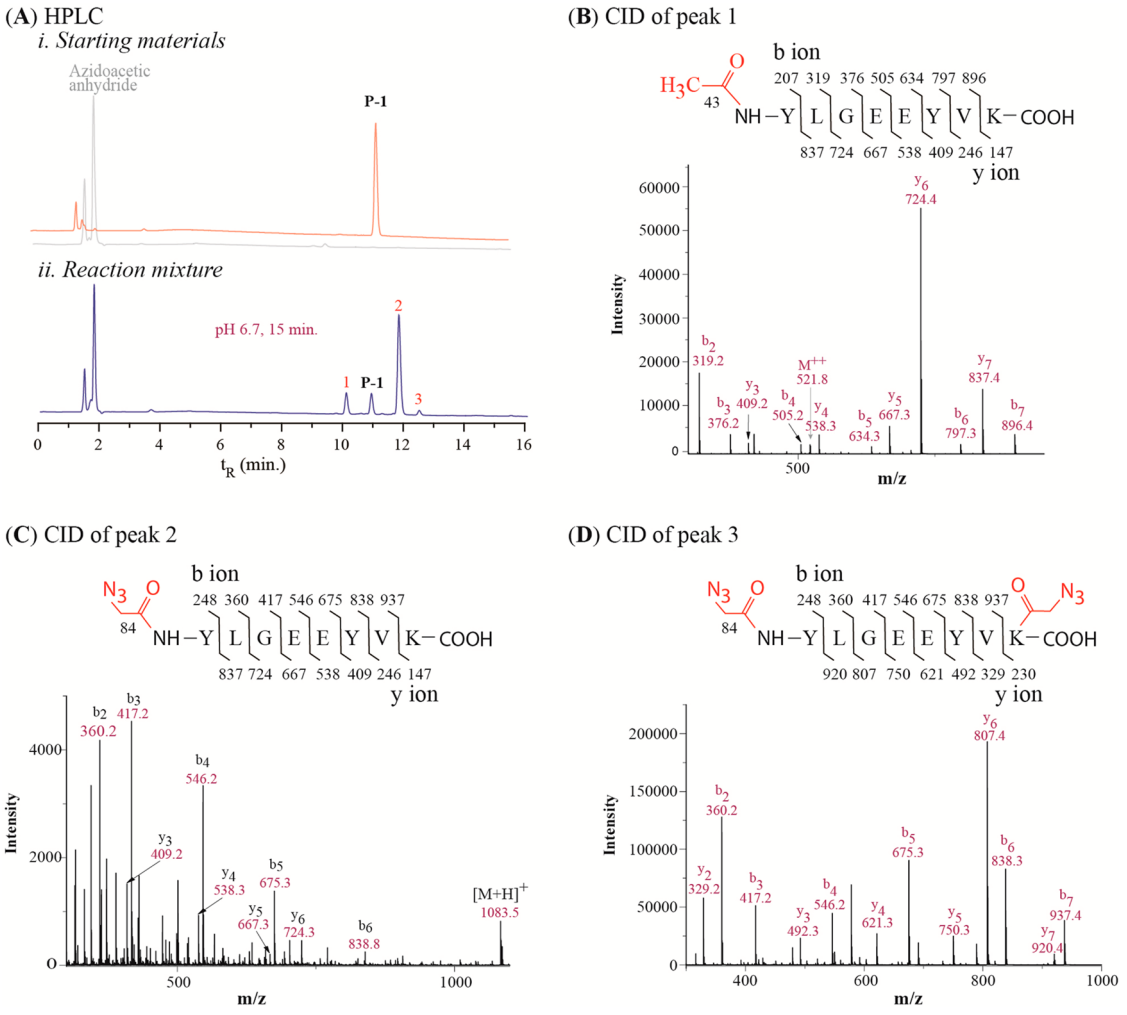

Figure 1. HPLC and Mass analysis of azidoacetic anhydride reacting with P-1: (A) RP HPLC chromatograms of (*i*) starting materials and (*ii*) the reaction mixture at pH 6.7; (B) Tandem mass spectrum of peak 1 in (A); (C) Tandem mass spectrum of peak 2 in (A); (D) Tandem mass spectrum of peak 3 in (A); Inserts in B, C, and D are calculated fragment ions of the corresponding peptides. See Table S1 in Supporting Information for detailed analysis of tandem mass data from collisional-induced dissociation (CID).

concentration of 0.4 mM and azidoacetic anhydride at 1.2 mM in a sodium acetate buffer, pH 6.7 at 0 °C, and monitored by reverse phase (RP) HPLC. The retention time (t_R) of each starting material was determined by a separate HPLC run (Figure 1, A-*i*). After 15 min, three new peaks appeared in the HPLC chromatogram, labeled as 1, 2, and 3 in red (Figure 1, A-*ii*). Peak 1 has a shorter retention time (t_R) than **P-1**; in contrast, both peak 2 and 3 have longer retention times compared to **P-1**. The ratio of these three peaks was 5:89:6, determined by their chromatographic peak areas. We separated these individual products and characterized them with MALDI and tandem mass spectrometry. Peak 1 was determined to be a product resulting from adding a 43 Da mass unit to **P-1**. In its CID spectrum (Figure 1, B), the mass of observed y ions (y3 to y7) matches those calculated from **P-1** without modification from its C-terminus to the amino acid residue next to the N-terminus, indicating that the reaction took place at the N-terminus. The N-terminal modification was further confirmed by observed b ions (Figure 1, B), each of them matching up with the mass derived from a **P-1** fragment plus an additional 42 Da. The 42 Da mass may be explained by substituting an acetyl group for one hydrogen of the α-amine (CH_3CO-H). To prove this substitution, we carried out a reaction of acetic anhydride with **P-1** under the same conditions, finding out that the major product (98%) had the same t_R and mass as the peak 1 (Figure S2, Supporting Information). This acetyl byproduct was unexpected, albeit only ~5% in the product mixture (and not reactive in the following reaction). Further investigations are required to determine its origin. Peak 2, which was the major product, has a mass of 1083.5 Da, corresponding to monoazidoacetylated **P-1**. By analyzing its CID spectrum, peak 2 was identified as a product of α-amine azidoacetylated **P-1** (Figure 1, C). Peak 3 has a mass of 1166.5, corresponding to the addition of two azidoacetyl groups to **P-1**, and its CID spectrum indicates that it is a product of both N-terminal and ε-lysine amine

azidoacetylated **P-1** (Figure 1, D). The data also show that the tyrosine residue did not react with azidoacetic anhydride below neutral pH. Next, we studied effects of pH and reaction time on products by means of HPLC analysis, and the results are listed in Table 2. First of all, at a pH below 7, azidoacetic anhydride reacted with the N-terminal amine with high selectivity (>90%). The selectivity increased by decreasing the pH, but the conversion of **P-1** to products was reduced as well. Extending the reaction time increased the conversion rate of peptide to products but also reduced the selectivity, and more byproducts were produced. Overall, the reaction of azidoacetic anhydride with **P-1** can achieve >90% selectivity and a > 90% conversion rate of starting material to product. Meanwhile, we tested PCA by reacting with **P-1** under the conditions reported in the literature, finding that it was less reactive and selective than azidoacetic anhydride based on the MALDI mass analysis of the reaction mixtures (Figure S3).

In turn, we examined the possible reaction of azidoacetic anhydride with histidine. **P-2** was a peptide adopted from hormone angiotensin II, carrying two histidine residues and no lysine in the sequence.

TABLE 2. Effects of Reaction Conditions on the Selectivity of Azidoacetic Anhydride

pH	time (min)	conversion of P-1	acylating ratio[a] (α to ε amine)
5.5	15	15%	100:0
6.1	15	61%	98.9:1.1
6.7	15	85%	96:4
6.7	60	97%	91:9

[a] Calculated based on areas of peak 2 and 3.

At pH 6.7, it reacted with azidoacetic anhydride, resulting in three products (Figure 2, A-*i*, labeled as 1, 2, 3 in red). Their ratio was determined to be 91:5:4, in which peak 1 was the major product. The CID mass analysis confirmed that the peak 1 was a product of N-terminal azidoacetylated **P-2**, and that both peak 2 and peak 3 were products of **P-2** with one of its histidine residues azidoacetylated (see Figure S4 in Supporting Information). When lowering the reactant ratio to 3:1 between azidoacetic anhydride and **P-2**, the conversion rate was reduced to 17%, but the product ratio between peak 1 and 2 was 91:9 and peak 3 did not appear (Figure 2, A-*ii*). At pH 5.5, peak 2 became a major product (Figure 2, A-*iii*). This is probably because the imidazolyl ring of histidine has a lower pK_a than the N-terminus amine so that it is more reactive at the low pH. Unexpectedly, the azidoacetyl group on the imidazolyl ring could not be removed by a base treatment (even with concentrated ammonia). Thus, the α-amine acylation at pH ∼ 6.7 minimizes the histidine side reaction.

To further explore limitation of the acylation reaction, we studied the reaction of azidoacetic anhydride with **P-3**, which has three lysine residues at its C-terminus. As a result, **P-3** yielded a mixture of five new products at pH 6.7, labeled as 1, 2, 3, 4, 5 in red, respectively (Figure 2, B-*i*). We assigned these peaks to their corresponding products in the same way as was done for **P-1**. The peak 1 is a product resulting from **P-3** with the N-terminal α-amine acetylated, peak 2 is a product of **P-3** with one lysine azidoacetylated, peak 3 is **P-3** with N-terminal α-amine azidoacetylated, and peaks 4 and 5 are **P-3** with two lysine azidoacetylated

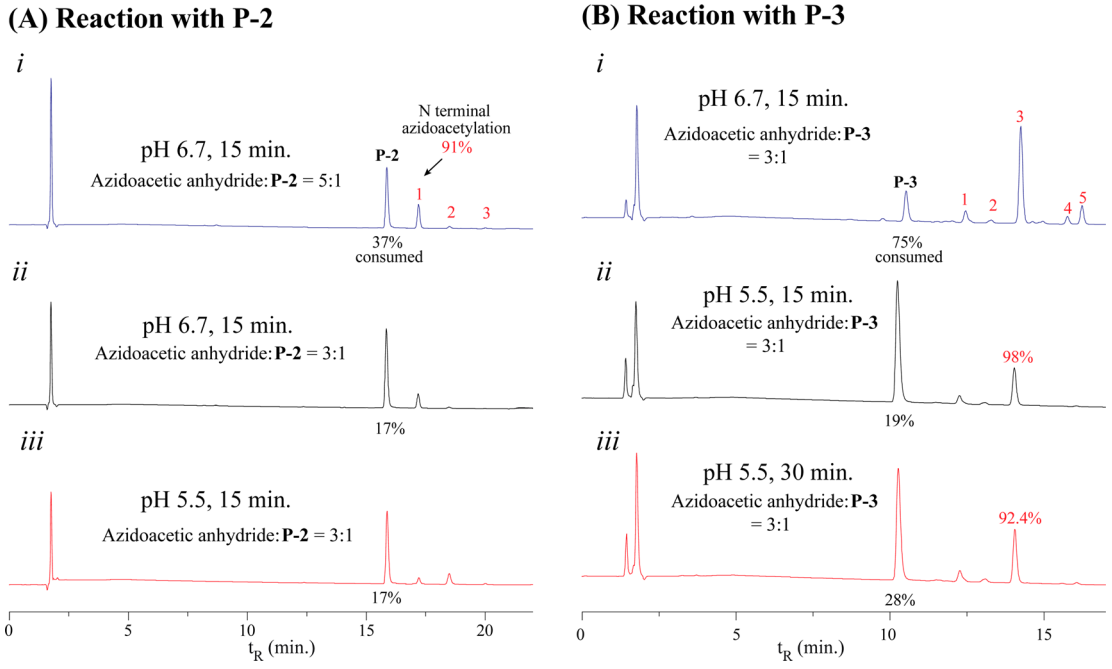

Figure 2. RP HPLC profiles of azidoacetic anhydride reacting with P-2 (A) and P-3 (B) at different pH and reaction time with temperature at 0 °C.

(Figure S5, Supporting Information). We determined the ratio of peak 1:2:3:4:5 = 7.1:2.2:73.0:5.0:12.7. Again, the N-terminal azidoacetylated product (peak 3) was the major product. This result shows that the azidoacetylating reaction can selectively take place at the N-terminal α-amine of a peptide containing multiple lysine residues, but its selectivity will be reduced. We studied the pH effects on the reaction. As shown in Figure 2, B-*ii*, the selectivity increased to ~98% at pH 5.5, but the conversion rate of the peptide-to-product was reduced to 19% from 75% at pH 6.7. Comparing the result shown in B-*ii* with that in B-*iii* of Figure 2 can deduce that extending the reaction time increases the conversion rate of peptide-to-product, and reduces the selectivity in the meanwhile. In brief, the azidoacetic anhydride reagent can rapidly react with α-amine with high selectivity under slightly acidic conditions, suitable for labeling the N-termini of trypsin digests.

Next, we studied the reaction of *N*-azidoacetylated peptides with PolyT_{20} (Step 2 in Scheme 1). ADIBO-T_{20} was synthesized by reacting DBCO-NHS ester with PolyT_{20} bearing a C12 amino modifier at its 5′-end in a phosphate buffer at pH 8, and purified by RP HPLC (see Methods and Figure S6 in Supporting Information). It spontaneously reacted with each of *N*-azidoacetylated peptides when they were mixed in a TEAA buffer (pH 7), resulting in the desired peptide-PolyT_{20} conjugates (designated as **P-1-T_{20}**, **P-2-T_{20}**, and **P-3-T_{20}**), which were characterized by MALDI mass spectrometry. The HPLC analysis indicated that these peptides were quantitatively converted to the corresponding peptide-PolyT_{20} conjugates with no detectable byproducts (Figure S7, Supporting Information). Nonetheless, the times to complete these reactions were different among these peptides, 45 min for reacting with *N*-azidoacetylated **P-1**, 20 min with azidoacetylated **P-2**, and 10 min with azidoacetylated **P-3**. The reaction rates seem to correlate with net charges of these peptides (see Table 1). The more positively charged **P-3** reacted with the negatively charged PolyT_{20} fastest, the negatively charged **P-1** the slowest, and **P-2** (which has a smaller positive charge) was intermediate. We also noticed that the product peaks are split into two or broadened in the HPLC chromatograms. This is because the ADIBO-azide reaction produces two triazolyl regioisomers, to which a peptide is connected either at the position 1 or 3 of the triazole rings (see Scheme 1). In the same manner, we have synthesized a conjugate of **P-1-T_{20}-3′** with **P-1** attached to 3′-end of Poly-T_{20} (Supporting Information). We also characterized these conjugates with CD spectroscopy (Figure 3). At first glance, these CD spectra are dominated by signature of DNA. Compared to polyT_{20} modified with ADIBO, the negative peaks (at ~250 nm) of the conjugates are reduced, with their intensities in an order: **ADIBO-T_{20}** > **P-2-T_{20}** ≈ **P-1-T_{20}-3′** > **P-1-T_{20}** > **P-3-T_{20}**.

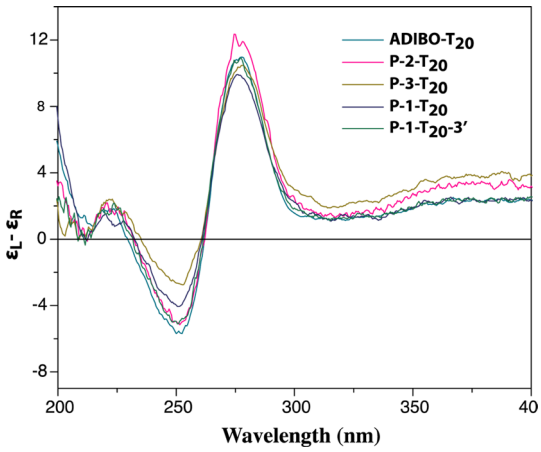

Figure 3. CD spectra of polyT_{20}-peptide conjugates. The measurement was carried out with each analyte in a 50 μM concentration in a sodium acetate buffer, pH 6.7. Each curve was an average of 4 scans with the buffer as a reference.

This may reflect the lysine residue at the C-termini interacting with the phosphate backbone when the peptide is conjugated to the 5′-end of PolyT_{20}, resulting in diminished helical structure. **P-3-T_{20}** containing three lysine residues at its C-termini has the strongest interaction with PolyT_{20} and so the smallest intensity at 250 nm.

Translocation of Peptide-PolyT_{20} Conjugates through Solid-State Nanopores. We used the setup illustrated in Figure 4-A to measure the molecular translocation, following a procedure we previously reported on measurements of DNA translocation through solid-state nanopores.[45] In more detail, a silicon chip containing a nanopore drilled by TEM was mounted in a homemade PTFE/PCTFE cell and sealed with a silicone elastomer gasket to form two separate chambers. The analyte solution was loaded in the *cis*-side of the nanopore where the electrode was grounded, with a final concentration of ~1.0 μM. All of measurements were carried out in a 0.4 M KCl electrolyte solution buffered with 1.0 mM phosphate buffer, pH 7.4. Figure 4-B shows three typical nanopores we used for the translocation measurements. Their sizes and shapes are slightly different from one another, as determined by TEM imaging. The measured conductances of Pore 2 and 3 are slightly smaller than calculated values (Figure 4-B)[46] probably because of their nonuniformed shapes. With each individual nanopore, we were able to finish measurements on translocation of a peptide-PolyT_{20} conjugate as well as its parent peptide and oligonucleotide before the pore became clogged. In a typical translocation experiment, we made measurements in the following order: PolyT_{20}, peptide-PolyT_{20} conjugate, peptide, and followed by a repeated measurement of PolyT_{20}. Between the measurements, the nanopore was rinsed with the electrolyte solution to remove any analyte residue and restore it to the original conductive state. The raw data generated by these

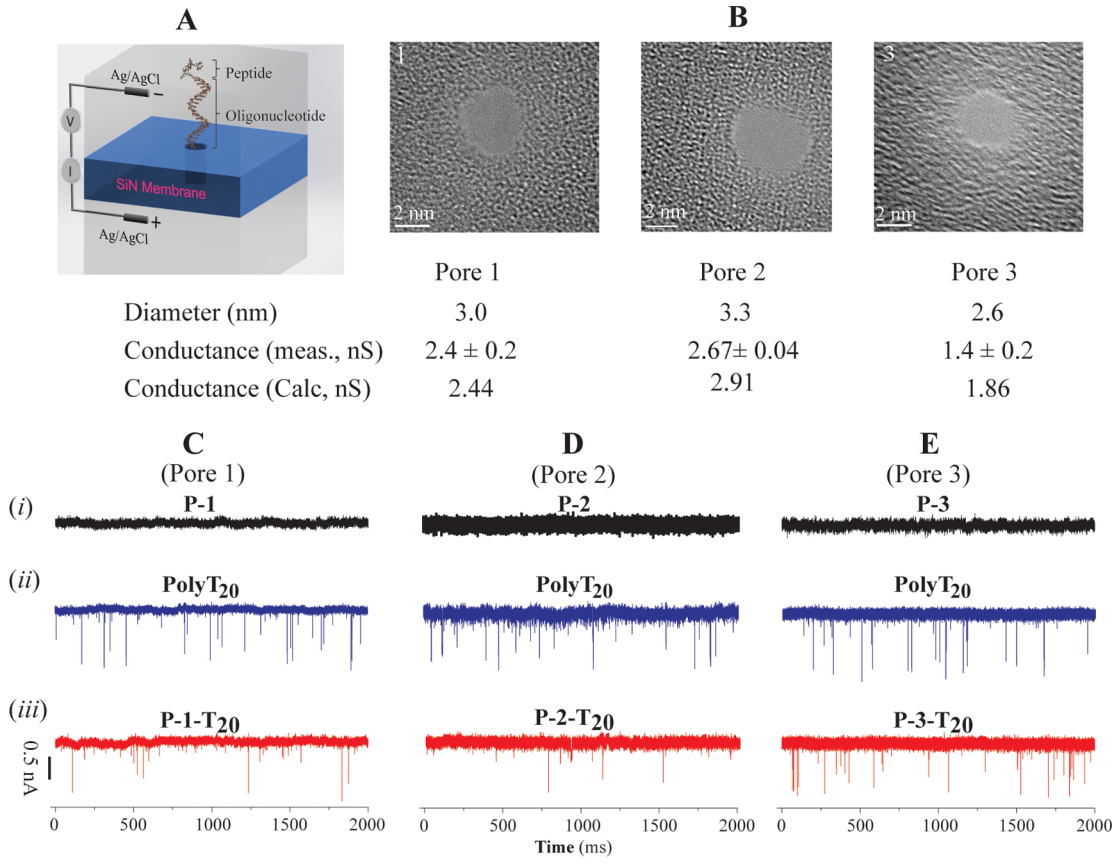

Figure 4. (A) Schematic illustration of a nanopore device for translocation measurements; (B) TEM images of the nanopores used for translocation and their physical parameters; (C) Ionic current traces of *i*: P-1, *ii*: PolyT$_{20}$, *iii*: P-1-T$_{20}$ in Pore 1; (D) Ionic current traces of *i*: P-2, *ii*: PolyT$_{20}$, *iii*: P-2-T$_{20}$ in Pore 2; (E) Ionic current traces of *i*: P-3, *ii*: PolyT$_{20}$, *iii*: P-3-T$_{20}$ in Pore 3 (Bias: 500 mV; Analyte concentration: ~1.0 μM).

nanopores are shown in Figure 4-C (Pore 1), D (Pore 2), and E (Pore 3), respectively. One can immediately notice that there was no translocation of peptides because neither negatively charged **P-1** nor positively charged **P-2** and **P-3** created current blockade spikes (Figure 4, C-*i*, D-*i*, and E-*i*) under our measurement conditions. Although Lee and co-workers reported that charged short peptides translocated through protein nanopores and blocked the ion current,[47,48] the concentrations they used were 50 to 100 times higher than what we used here. As expected, PolyT$_{20}$ was readily translocated through these nanopores (Figure 4, C-*ii*, D-*ii*, and E-*ii*). The peptide-PolyT$_{20}$ conjugates all gave frequent blockade signals, indicating that they translocated too (Figure 4, C-*iii*, D-*iii*, and E-*iii*). Their translocation was further confirmed by reversing the bias across the nanopore. When doing this, we observed the blockade signals only after a significant time of translocating the conjugates in the forward direction, which strongly suggested that molecules were translocated through the pores (data not shown). Translocation was also confirmed by measuring the voltage dependence of the duration of the current blockade (see below).

These current spikes (examples are shown in Figure S8) were analyzed by means of the OpenNanopore software and each spike was assigned a dwell time and a current-blockade value. We found that the majority of translocation events were single-level blockades (>90% for PolyT$_{20}$ and ~95−97% for peptide-PolyT$_{20}$ conjugates) while only a small percentage of the events were multilevel blockades (~10% for PolyT$_{20}$ and ~3−5% for peptide-PolyT$_{20}$ conjugates). In comparison, the multilevel events occurred rarely with PolyT$_{20}$ and even less so with the peptide-PolyT$_{20}$ conjugates, which may be partially explained by the difference between the 5′ and 3′ end threading of the PolyT$_{20}$ (further discussed below). Some typical scatter plots of dwell times *vs* current blockades for PolyT$_{20}$ and its peptide conjugates (at 500 mV bias) are shown in the panels labeled (i) in Figure 5. The dwell times of the translocation events were reduced with increased voltage bias (Figure S9 in Supporting Information). This observation is also consistent with molecular translocation as the origin of these blockade events. It has been reported that for a translocation event with a favorable electric field (*i.e.*, electrophoretically driven), the dwell time of a polymeric molecule in the nanopore decreases as the voltage increases.[48,49]

The distributions of dwell times for the Poly-T$_{20}$ and the peptide conjugates appear to be highly overlapped.

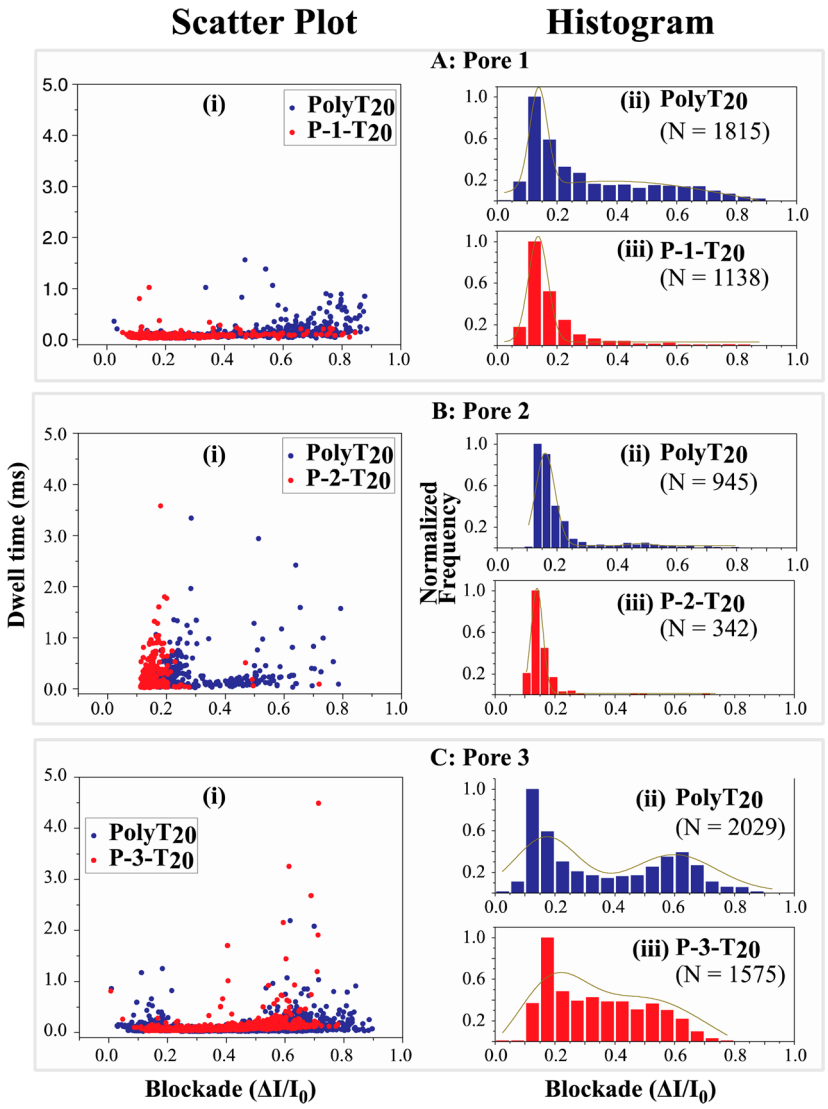

Figure 5. Scatter-plot of dwell time *vs* current blockade (i) and histograms of fractional current blockades for $PolyT_{20}$ (ii) and its peptide conjugates (iii) at bias =500 mV). (A) Translocation through Pore 1; (B) Translocation through Pore 2; (C) Translocation through Pore 3. Blue: $PolyT_{20}$, Red: peptide conjugate; $\Delta I = I_0$ (open pore current) $- I$ (blocked pore current). The dark yellow lines in histograms are the Gaussian fitting curves and *N* = number of events.

TABLE 3. Dwell Times of $PolyT_{20}$ and Its Peptide Conjugates in Different Nanopores

	pore 1		pore 2		pore 3		pore 4	
sample	$P\text{-}1\text{-}T_{20}$	$PolyT_{20}$	$P\text{-}2\text{-}T_{20}$	$PolyT_{20}$	$P\text{-}3\text{-}T_{20}$	$PolyT_{20}$	$P\text{-}1\text{-}T_{20}$	$P\text{-}1\text{-}T_{20}\text{-}3'$
exp. fit (μS)	38 ± 0	61 ± 1	64 ± 5	134 ± 13	86 ± 4	74 ± 1	75 ± 3	124 ± 3
mean (μS)	66	91	207	158	101	94	129	188
median (μS)	60	70	60	90	70	70	80	110

In the absence of complicating factors (such as interactions with the pore surface) the distribution of blockade times is described by a first-passage time distribution as given by Carson *et al.*[50] We have approximated this by an exponential distribution and fitted measured data for all three pores and the various conjugates (Figure S10). There are a significant number of very long blockades, so we have also listed the mean and medians of the blockade times in Table 3. The discrepancies between the three measures of the distributions are a measure of how widely the data are distributed. In addition, the distributions change from pore to pore, as can be seen by comparing values for $PolyT_{20}$ between the three pores. However, by most measures, we see the somewhat surprising result that the conjugates translocate more rapidly, or on

about the same time scale, as PolyT$_{20}$ alone (data for Pores 1 to 3).

Data for the current blockades give a clearer picture of the differences between PolyT$_{20}$ and its peptide conjugates than the widely distributed translocation times. In order to compare data for the various samples, each blockade-current data set was normalized by its maximum value and plotted into a normalized histogram, as shown in Figure 5 (panels labeled as (ii) for PolyT$_{20}$, and panels labeled as (iii) for its peptide conjugates). We consider first the PolyT$_{20}$ data. All the data sets were fitted by a double-peaked Gaussian function with $R^2 > 0.90$ (panel (ii)'s in Figure 5), with a major peak at $\Delta I/I_0$ in the range of 0.15 to 0.2 and a minor peak in the range of 0.5 to 0.6. Similar features have been reported for DNA translocation through α-hemolysin pores where they were explained by the so-called Christmas-tree effect.[51,52] When a single stranded DNA is translocated, it can thread either *via* its 5′- or its 3′-end into a nanopore. Meller and co-workers demonstrated by all-atom molecular dynamics (MD) that DNA bases in a stretched conformation preferably tilt toward the 5′-end in a confined pore.[51] This is because all of nucleosides in DNA have a β configuration, in which a nucleobase stays at the same side with the 5′-hydroxyl group of a nucleoside on the deoxyribose ring. As a result, DNA translocation with threading through the 3′-end should be more frequent and less blockaded than through the 5′-end (just as a Christmas tree can be moved into a door more easily from its trunk end than from its tip). Based on this hypothesis, we may assign the major blockade peaks (at smaller current values) for translocation events through the 3′-end threading. From the literature, we found a similar trend in the translocation of PolyA$_{20}$ through a α-HL nanopore.[53] Thus, when a short peptide is tethered to the 5′-end of PolyT$_{20}$, it reduces the probability of threading through the 5′-end. This accounts for the observation that the large current blockades were diminished in the translocation of the peptide-PolyT$_{20}$ conjugates, such as in panel (iii)'s of Figure 5-A and -B, compared to the corresponding PolyT$_{20}$. **P-3-T$_{20}$** displays a large tail following its major peak (panel (iii) in Figure 5-C) and also translocates more slowly (Table 3) than the other two conjugates just mentioned above. This might be explained by the conformational structure of the peptide-PolyT$_{20}$ conjugate. The CD spectrum (Figure 3) shows that the peptide **P-3** has stronger interactions with the backbone of PolyT$_{20}$ in the conjugate than other two peptides, which may result in looped structures. When a conjugate with such a structure translocates through the nanopore, it would create larger blockade currents, as observed.

To further verify the Christmas-tree effect, we synthesized a conjugate **P-1-T$_{20}$-3′**, in which **P-1** is tethered to the 3′-end of PolyT$_{20}$ and compared its translocation with that of **P-1-T$_{20}$**, in which **P-1** is tethered to the 5′-end of PolyT$_{20}$ (illustrated in Figure 6-A), in a nanopore with a diameter of ~3.2 nm (Pore 4 in Figure 6-B). From Figure 6-C, one can immediately see that **P-1-T$_{20}$** was translocated through the nanopore much more frequently than **P-1-T$_{20}$-3′**. From data collected over a 2000 ms period for both conjugates, we find that that the **P-1-T$_{20}$** was translocated 5 fold more frequently than **P-1-T$_{20}$-3′** (337 *vs* 66 events). These two sets of data were normalized in the same manner as was done for those in Figure 5, plotted into histograms separately, and then fitted with a double peak Gaussian function (Figure 6, D). As expected, **P-1-T$_{20}$** shows a preference for threading into the nanopore from the 3′-end of PolyT$_{20}$ with a major blockade peak at $\Delta I/I_0 = 0.09$ (Figure 6-D, (i). Similarly, **P-1-T$_{20}$-3′** also shows a major blockade peak at $\Delta I/I_0 = 0.11$ (Figure 6-D, (ii), indicating that it still entered the nanopore mainly through the 3′-end of PolyT$_{20}$, despite being blocked by peptide tethered at that end. This may be explained by the Christmas-tree effect, which results in a strong tendency for DNA to translocate through the 3′-end threading. Since **P-1** is relatively short and negatively charged, it would not be able to completely block the 3′-end threading and only reduced the translocation frequency when it was tethered to the 3′-end of PolyT$_{20}$. Dwell times for the two conjugates are summarized under the column Pore 4 in Table 3, distributions of which are well fitted into an exponential decay function (Figure S11). All three measures of the distribution indicate that **P-1-T$_{20}$** translocated faster as the conjugate entered more probably at the 3′-end. The small fraction of multilevel events may be at least partially explained by the Christmas-tree effect. The multilevel events occurred mostly in higher current blockade signals (panel I and J in Figure S8) and were reduced from ~10% with PolyT$_{20}$ to ~3−5% with the peptide-PolyT$_{20}$ conjugates. Since a lower front step exists in these multilevel events, we attribute them to the resistance to entry of the pore from the 5′-end of PolyT$_{20}$. Given the "Christmas-tree effect", we conclude that the attachment of peptides to 5′-end of an oligonucleotide is an optimal choice for the nanopore translocation.

CONCLUSIONS

The objective of this present study was to develop a simple and effective chemistry to functionalize peptides with a charged threading molecule to facilitate their translocation through nanopores. We have harnessed an acylation reaction for rapid introduction of an orthogonal azido function to N-termini of peptides, which allowed us to quantitatively attach a charged oligonucleotide to peptides using a click reaction without the need of separating the intermediate products. At pH ~ 6.7 and 0 °C, azidoacetic anhydride quickly reacted with the α amine of a peptide containing one

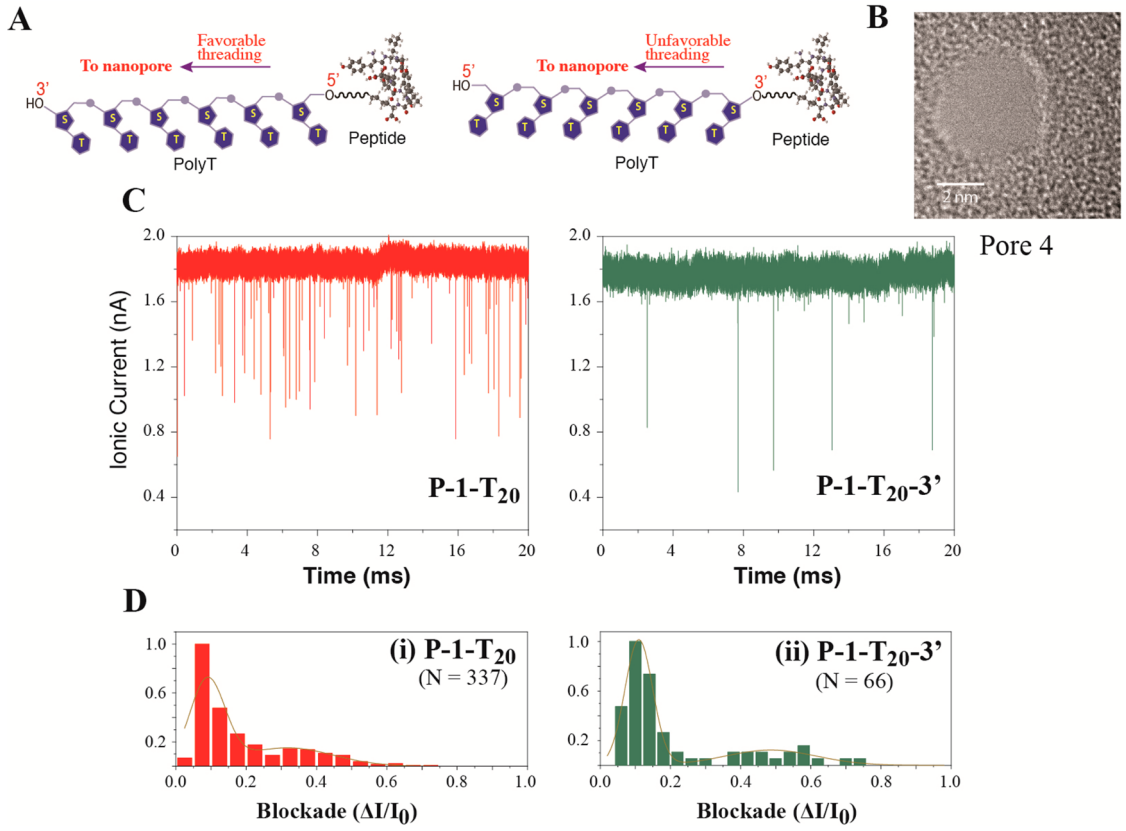

Figure 6. Testing the Christmas-tree effect in translocation of peptide-DNA conjugates. (A) Schematic illustration of peptide-PolyT$_{20}$ conjugates; (B) TEM images of the nanopores used for translocation; (C) Ionic current traces of peptide-PolyT$_{20}$ conjugates translocating through the nanopore; (D) Current blockade histograms of (i) P-1-T$_{20}$ and (ii) P-1-T$_{20}$-3′ with normalized data. The dark yellow lines in histograms are Gaussian fitting curves, and *N* = number of events.

lysine residue with >90% selectivity, and the side reaction with imidazolyl ring of histidine was reduced to a minimum. Thus, our chemistry should be practical for use in preparing peptides sample obtained from trypsin digests for nanopore analysis. Because of the reduced selectivity (~80%) in reacting with a peptide containing three lysine residues, further improvements are required if the method is to be applied more widely to peptides from other sources.

Furthermore, we have shown that the peptide-PolyT$_{20}$ conjugates can effectively translocate through solid-state nanopores, which lays down a foundation for us to develop a technique for analysis of proteins using nanopores. Our data indicate that an oligonucleotide, such as PolyT$_{20}$ can be used as an effective molecular thread to carry peptides through solid-state nanopores, its conjugates preferentially entering the nanopore from the 3′-end. While the sensitivity of ion-current measurements is unlikely to be adequate for *de novo* sequencing, it is clear that structural aspects of peptides can be probed using the translocation of conjugates. We hope to integrate this technology with recognition tunneling in order to explore the possibility of sequencing with single amino acid resolution in the future.[10]

METHODS

General Information. Chemicals were purchased from Sigma-Aldrich and anhydrous organic solvents were Aldrich's Sure/Seal. ADIBO-NHS ester was purchased from Click Chemistry Tools. Peptides were custom synthesized by CPC Scientific (San Jose, CA, USA) and oligonucleotides (PolyT$_{20}$) with an amino modifier at its 5′- or 3′-end by IDT (Integrated DNA Technologies). ^{1}H and ^{13}C NMR spectra were recorded at 400 MHz (^{1}H), 100 MHz (^{13}C), respectively. Chemical shifts are given in parts per million (ppm) on the delta scale (δ) and are referred to the solvent residual peak. HPLC analysis and purification were carried out in Agilent 1100 series equipped with a UV detector and a fraction collector. A Zorbax Eclipse Plus C18 column (4.6 × 150 mm, particle size 5 μm) from Agilent was used for the reversed phase HPLC. MALDI-TOF analysis was performed on Voyager-DE STR instrument.

Azidoacetic Anhydride. The synthesis was carried out following a method reported in literature with modification.[54] *N*,*N*′-Dicyclohexylcarbodiimide (DCC, 204 mg, 0.98 mmol) was added to a solution of 2-azidoacetic acid (200 mg, 1.98 mmol) in anhydrous tetrahydrofuran (2 mL). The solution was stirred for 2 h and 15 min, during which the precipitate was gradually produced, and filtered. The filtrate was concentrated by rotary evaporation, giving azidoacetic anhydride (150 mg, 42%) as a colorless liquid. ^{1}H NMR (400 MHz, $CDCl_3$) δ: 3.85 (s, 4H); ^{13}C NMR (100 MHz, $CDCl_3$) δ: 168.3, 50.0.

General Procedure for Reaction of Azidoacetic Anhydride with Peptides (P-1, P-2, and P-3). A solution of azidoacetic anhydride in acetonitrile (5 mM, 3.0 μL) was added to a solution of peptide in a

50 mM sodium acetate buffer (0.5 mM, 10 μL) with a predefined pH value in an eppendorf tube. The reaction was kept at 0 °C for 15 min, followed by the addition of water (10 μL), and remaining the reaction in ice for another 10 min for completely terminating the reaction. RP HPLC, with a gradient of 5 to 45% B in 25 min (solvent A: 0.1 M TEAA buffer, pH 7.0; solvent B: acetonitrile), was used to monitor the reactions and separate products.

Functionalization of PolyT_{20} with ADIBO. A solution of PolyT_{20} containing a C12 amino modifier at its 5′-end (1 mM, 10 μL) in water and ADIBO-NHS ester in DMSO (15 mM, 80 μL) were mixed in a phosphate buffer (30 μL, pH 8). The solution was shaken for 20 min at room temperature. The product (**ADIBO-T_{20}**) was purified by RP HPLC in a Zorbax Eclipse Plus C18 column (4.6 × 150 mm, particle size 5 μm) with a gradient of 10 to 60% B in 25 min (solvent A: 0.1 M TEAA buffer, pH 7.0; solvent B: acetonitrile). MALDI-TOF-MS calc. for [$C_{233}H_{304}N_{42}O_{143}P_{20}$] (M + H): *m/z* 6600.58; found: 6603.34.

Reaction of *N*-Azidoacetylated P-1 with ADIBO-T_{20}. A solution of *N*-azidoacetylated **P-1** (30 μM, 15 μL) in a TEAA buffer (50 mM, pH 7) was mixed with ADIBO-T_{20} (30 μM, 15 μL) in the TEAA buffer (50 mM, pH 7), and shaken at room temperature for 45 min. RP HPLC analysis showed the starting material was consumed. The product **(P-1-T_{20})** was purified by RP HPLC in a Zorbax Eclipse Plus C18 column (4.6 × 150 mm, particle size 5 μm) with a gradient of 10 to 60% B in 25 min (solvent A: 0.1 M TEAA buffer, pH 7.0; solvent B: acetonitrile). After lyophilization, the product was given as a white powder. MALDI-TOF-MS calc. for [$C_{282}H_{374}N_{54}O_{159}P_{20}$] (M + H): *m/z* 7683.12; found: 7684.72.

Reaction of *N*-Azidoacetylated P-2 with ADIBO-T_{20}. A solution of *N*-azidoacetylated **P-2** (30 μM, 15 μL) in a TEAA buffer (50 mM, pH 7) was mixed with ADIBO-T_{20} (30 μM, 25 μL) in the TEAA buffer (50 mM, pH 7), and shaken at room temperature for 20 min, purified by RP HPLC under the same conditions as did for **P-1-T_{20}**. After lyophilization, the product (**P-2-T_{20}**) was given as a white powder. MALDI-MS calc. for [$C_{297}H_{394}N_{62}O_{158}P_{20}$] (M + H): 7979.31; found: 7978.64).

Reaction of *N*-Azidoacetylated P-3 with ADIBO-T_{20}. A solution of *N*-azidoacetylated **P-3** (30 μM, 15 μL) in a TEAA buffer (50 mM, pH 7) was mixed with ADIBO-T_{20} (30 μM, 15 μL) in the TEAA buffer (50 mM, pH 7), and shaken at room temperature for 10 min, purified by RP HPLC under the same conditions as did for **P-1-T_{20}**. After lyophilization, the product (**P-3-T_{20}**) was given as a white powder. MALDI-MS calc. for [$C_{299}H_{406}N_{60}O_{160}P_{20}$] (M + H): *m/z* 8019.39; found: 8020.58.

Tandem Mass Spectrometry. Collisional-induced dissociation (CID) and subsequent mass analysis of modified peptides were carried out on a Bruker MaXis 4G quadrupole-time-of-flight (Q-TOF) mass spectrometer equipped with a microflow nebulizer electrospray ionization (ESI) source operated in positive ion mode. HPLC-purified peptide samples were diluted to a final concentration of approximately 20 μM in a 50/50 mixture of acetonitrile/water containing 0.1% (v/v) formic acid. Prior to analysis, the TOF mass analyzer was externally calibrated with a tuning mixture supplied by Agilent containing 10 species of varying but equally spaced masses from 118 to 2722 Da. Peptide solutions were infused into the ion source by syringe pump at a rate of 1.0 μL/min. The end plate offset and capillary were set to potentials of 500 V and 4,500 V, respectively. The nebulizer gas and the dry gas (both N_2) were set to 1.4 bar and 4.0 L/min, respectively, and the dry gas temperature was set to 220 °C. The RF amplitude on ion funnel 1 and the multipole were both set to 400 Vpp. No in-source CID energy was used. Quadrupole ion energy was set to 3.0 eV. Precursor ions were selected with an *m/z* width of 2 and imparted enough energy (usually 10−40 eV) to diminish the relative abundance of the precursor ion to less than 5%. Spectral digitization was set to a rate of 4 GHz and individual TOF transients were summed and recorded at a rate of 1 Hz. After equilibration and spray stabilization, each mass spectrum was recorded for 1.5 min, and then averaged into a single spectrum.

Fabrication of Nanopores. Silicon chips (5 × 5 mm) coated with silicon nitride (30 nm thick) from Norcada Inc. were used for the fabrication of nanopores. First, a 250 × 250 μm SiN_x window was opened from the Si backside of the chip and the thickness of free-standing SiN_x membrane left was 30 nm. After standard cleaning process, nanopores were drilled using the electron beam in JEOL 2010FEG transmission electron microscope (TEM) at 200 kV. The size of the pores were controlled by the electron beam and monitored using the TEM CCD. The nanopores were imaged right after drilling.

Translocation Measurements. Prior to a translocation experiment, a nanopore chip was immersed in hot piranha (H_2O_2:H_2SO_4 = 1:3) for 10 min, and then rinsed with water. After drying with a N_2 flow, the nanopore chip was assembled in a piranha-cleaned PCTFE cell to form the *cis* reservoir, and sealed with a quick-curing silicone elastomer gasket for reduced capacitance. The PCTFE cell with a nanopore chip was then assembled with PTFE base to form the *trans* reservoir. Electrolyte solution used was 0.4 M KCl in 1 mM phosphate buffer (pH 7.4), which was filtered with a Millipore 0.2 μm filter. Ag/AgCl electrodes, made from fresh Ag wires with bleach, were inserted into both *cis* and *trans* sample reservoirs for ionic current measurement. All of analytes were dissolved in the electrolyte solution for the nanopore analysis.

The electrolyte solution was used as a translocation reference. Each translocation experiment began with filling the electrolyte solution in both reservoirs and running the reference to ensure a steady baseline current and no electrical spikes. Then, an analyte solution was injected into the *cis* reservoir with a final concentration of 0.5−1 μM. A translocation bias was applied to the Ag/AgCl electrode in the *trans* reservoir, while the electrode in the *cis* reservoir was kept grounded to avoid adsorption of analyte molecules. After recording the ionic current, the *cis* reservoir was drained and rinsed with the buffer solution. Another baseline was recorded to ensure no contaminations left in *cis* reservoir before a new analyte solution was injected.

Data Collection and Analysis. Ionic currents were collected at a 100 kHz sampling rate with a 10 kHz low pass filter using patch clamp amplifier Axon Axopatch 200B, with digitizer DigiData 1550A from Axon Instruments Inc. PClamp 10.4 software and an in-house developed LabView program were used for recording the ionic current data. The data were analyzed using MATLAB based software OpenNanopore, developed by Laboratory of Nanoscale Biology (LBEN) of École Polytechnique Fédérale de Lausanne (EPFL). OpenNanopore fits abrupt stepwise signals in the presence of Gaussian noise with a level threshold of 200 pA. Statistic analysis was carried out in OriginPro 2015, in which the Levenberg−Marquardt algorithm was used for Gaussian fitting.

Conflict of Interest: The authors declare the following competing financial interest(s): PZ, SL, and SB are named as inventors on related patent applications.

Acknowledgment. This work was supported in part by a DNA sequencing technology grant from the NHGRI (HG 006323). We would like to thank Professor M. Wanunu of Northeastern University for his suggestions and advice on nanopore translocation experiments.

Supporting Information Available: The Supporting Information is available free of charge on the ACS Publications website at DOI: 10.1021/acsnano.5b04984.

Supporting tables and figures, and synthesis of **P-1-T_{20}-3′**.

REFERENCES AND NOTES

1. Laszlo, A. H.; Derrington, I. M.; Ross, B. C.; Brinkerhoff, H.; Adey, A.; Nova, I. C.; Craig, J. M.; Langford, K. W.; Samson, J. M.; Daza, R.; Doering, K.; Shendure, J.; Gundlach, J. H. Decoding Long Nanopore Sequencing Reads of Natural DNA. *Nat. Biotechnol.* **2014**, *32*, 829–833.
2. Oukhaled, A.; Bacri, L.; Pastoriza-Gallego, M.; Betton, J. M.; Pelta, J. Sensing Proteins through Nanopores: Fundamental to Applications. *ACS Chem. Biol.* **2012**, *7*, 1935–1949.
3. Fennouri, A.; Przybylski, C.; Pastoriza-Gallego, M.; Bacri, L.; Auvray, L.; Daniel, R. Single Molecule Detection of Glycosaminoglycan Hyaluronic Acid Oligosaccharides and Depolymerization Enzyme Activity Using a Protein Nanopore. *ACS Nano* **2012**, *6*, 9672–9678.

4. McMullen, A.; de Haan, H. W.; Tang, J. X.; Stein, D. Stiff filamentous Virus Translocations through Solid-State Nanopores. *Nat. Commun.* **2014**, *5*, 4171.
5. Reiner, J. E.; Balijepalli, A.; Robertson, J. W.; Campbell, J.; Suehle, J.; Kasianowicz, J. J. Disease Detection and Management *via* Single Nanopore-Based Sensors. *Chem. Rev.* **2012**, *112*, 6431–6451.
6. Pennisi, E. DNA Sequencers Still Waiting for the Nanopore Revolution. *Science* **2014**, *343*, 829–830.
7. Mikheyev, A. S.; Tin, M. M. A First Look at the Oxford Nanopore MinION Sequencer. *Mol. Ecol. Resour.* **2014**, *14*, 1097–1102.
8. Ashton, P. M.; Nair, S.; Dallman, T.; Rubino, S.; Rabsch, W.; Mwaigwisya, S.; Wain, J.; O'Grady, J. MinION Nanopore Sequencing Identifies the Position and Structure of a Bacterial Antibiotic Resistance Island. *Nat. Biotechnol.* **2015**, *33*, 296–300.
9. Jain, M.; Fiddes, I. T.; Miga, K. H.; Olsen, H. E.; Paten, B.; Akeson, M. Improved Data Analysis for the MinION Nanopore Sequencer. *Nat. Methods* **2015**, *12*, 351–356.
10. Zhao, Y.; Ashcroft, B.; Zhang, P.; Liu, H.; Sen, S.; Song, W.; Im, J.; Gyarfas, B.; Manna, S.; Biswas, S.; Borges, C.; Lindsay, S. Single-Molecule Spectroscopy of Amino Acids and Peptides by Recognition Tunnelling. *Nat. Nanotechnol.* **2014**, *9*, 466–473.
11. Ohshiro, T.; Tsutsui, M.; Yokota, K.; Furuhashi, M.; Taniguchi, M.; Kawai, T. Detection of Post-Translational Modifications in Single Peptides Using Electron Tunnelling Currents. *Nat. Nanotechnol.* **2014**, *9*, 835–840.
12. Krasniqi, B.; Lee, J. S. RNase A Does Not Translocate the Alpha-Hemolysin Pore. *PLoS One* **2014**, *9*, e88004.
13. Nivala, J.; Marks, D. B.; Akeson, M. Unfoldase-Mediated Protein Translocation Through an Alpha-Hemolysin Nanopore. *Nat. Biotechnol.* **2013**, *31*, 247–250.
14. Rodriguez-Larrea, D.; Bayley, H. Multistep Protein Unfolding during Nanopore Translocation. *Nat. Nanotechnol.* **2013**, *8*, 288–295.
15. Steen, H.; Mann, M. The ABC's (and XYZ's) of Peptide Sequencing. *Nat. Rev. Mol. Cell Biol.* **2004**, *5*, 699–711.
16. Picotti, P.; Aebersold, R. Selected Reaction Monitoring−Based Proteomics: Workflows, Potential, Pitfalls and Future Directions. *Nat. Methods* **2012**, *6*, 555–566.
17. Pang, P.; Ashcroft, B. A.; Song, W.; Zhang, P.; Biswas, S.; Qing, Q.; Yang, J.; Nemanich, R. J.; Bai, J.; Smith, J. T.; *et al.* Fixed-Gap Tunnel Junction for Reading DNA Nucleotides. *ACS Nano* **2014**, *8*, 11994–12003.
18. Venta, K.; Shemer, G.; Puster, M.; Rodriguez-Manzo, J. A.; Balan, A.; Rosenstein, J. K.; Shepard, K.; Drndic, M. Differentiation of Short, Single-Stranded DNA Homopolymers in Solid-State Nanopores. *ACS Nano* **2013**, *7*, 4629–4636.
19. Si, W.; Sha, J.; Liu, L.; Qiu, Y.; Chen, Y. Effect of Nanopore Size on Poly(dT)30 Translocation through Silicon Nitride Membrane. *Sci. China: Technol. Sci.* **2013**, *56*, 2398–2402.
20. Lee, M. H.; Kumar, A.; Park, K. B.; Cho, S. Y.; Kim, H. M.; Lim, M. C.; Kim, Y. R.; Kim, K. B. A Low-Noise Solid-State Nanopore Platform Based on a Highly Insulating Substrate. *Sci. Rep.* **2014**, *4*, 7448.
21. Lundblad, R. L. *Chemical Reagents for Protein Modification*, 4th ed.; CRC Press: Boca Raton, FL, 2014.
22. Chan, A. O.; Ho, C. M.; Chong, H. C.; Leung, Y. C.; Huang, J. S.; Wong, M. K.; Che, C. M. Modification of N-Terminal Alpha-Amino Groups of Peptides and Proteins Using Ketenes. *J. Am. Chem. Soc.* **2012**, *134*, 2589–2598.
23. Gilmore, J. M.; Scheck, R. A.; Esser-Kahn, A. P.; Joshi, N. S.; Francis, M. B. N-Terminal Protein Modification through a Biomimetic Transamination Reaction. *Angew. Chem., Int. Ed.* **2006**, *45*, 5307–5311.
24. Witus, L. S.; Netirojjanakul, C.; Palla, K. S.; Muehl, E. M.; Weng, C. H.; Iavarone, A. T.; Francis, M. B. Site-Specific Protein Transamination Using N-Methylpyridinium-4-Carboxaldehyde. *J. Am. Chem. Soc.* **2013**, *135*, 17223–17229.
25. MacDonald, J. I.; Munch, H. K.; Moore, T.; Francis, M. B. One-Step Site-Specific Modification of Native Proteins with 2-Pyridinecarboxyaldehydes. *Nat. Chem. Biol.* **2015**, *11*, 326–331.
26. Song, J.; Kim, H. J. Matrix-Assisted Laser Desorption/Ionization Mass Spectrometry Peptide Sequencing Utilizing Selective N-Terminal Bromoacetylation. *Anal. Biochem.* **2012**, *423*, 269–276.
27. Koehler, C. J.; Arntzen, M. O.; Strozynski, M.; Treumann, A.; Thiede, B. Isobaric Peptide Termini Labeling Utilizing Site-Specific N-Terminal Succinylation. *Anal. Chem.* **2011**, *83*, 4775–4781.
28. Debets, M. F.; van Berkel, S. S.; Schoffelen, S.; Rutjes, F. P.; van Hest, J. C.; van Delft, F. L. Aza-Dibenzocyclooctynes for Fast and Efficient Enzyme PEGylation *via* Copper-Free (3 + 2) Cycloaddition. *Chem. Commun.* **2010**, *46*, 97–99.
29. Baskin, J. M.; Prescher, J. A.; Laughlin, S. T.; Agard, N. J.; Chang, P. V.; Miller, I. A.; Lo, A.; Codelli, J. A.; Bertozzi, C. R. Copper-Free Click Chemistry for Dynamic *in vivo* Imaging. *Proc. Natl. Acad. Sci. U. S. A.* **2007**, *104*, 16793–16797.
30. Nojima, T.; Konno, H.; Kodera, N.; Seio, K.; Taguchi, H.; Yoshida, M. Nano-Scale Alignment of Proteins on a Flexible DNA Backbone. *PLoS One* **2012**, *7*, e52534.
31. Witte, M. D.; Cragnolini, J. J.; Dougan, S. K.; Yoder, N. C.; Popp, M. W.; Ploegh, H. L. Preparation of Unnatural N-to-N and C-to-C Protein Fusions. *Proc. Natl. Acad. Sci. U. S. A.* **2012**, *109*, 11993–11998.
32. Zimmerman, E. S.; Heibeck, T. H.; Gill, A.; Li, X.; Murray, C. J.; Madlansacay, M. R.; Tran, C.; Uter, N. T.; Yin, G.; Rivers, P. J.; *et al.* Production of Site-Specific Antibody-Drug Conjugates Using Optimized Non-Natural Amino Acids in a Cell-Free Expression System. *Bioconjugate Chem.* **2014**, *25*, 351–361.
33. Heuer-Jungemann, A.; Kirkwood, R.; El-Sagheer, A. H.; Brown, T.; Kanaras, A. G. Copper-Free Click Chemistry as an Emerging Tool for the Programmed Ligation of DNA-Functionalised Gold Nanoparticles. *Nanoscale* **2013**, *5*, 7209–7212.
34. Subramanian, N.; Sreemanthula, J. B.; Balaji, B.; Kanwar, J. R.; Biswas, J.; Krishnakumar, S. A Strain-Promoted Alkyne-Azide Cycloaddition (SPAAC) Reaction of a Novel EpCAM Aptamer-Fluorescent Conjugate for Imaging of Cancer Cells. *Chem. Commun.* **2014**, *50*, 11810–11813.
35. Winz, M. L.; Samanta, A.; Benzinger, D.; Jaschke, A. Site-Specific Terminal and Internal Labeling of RNA by Poly(A) Polymerase Tailing and Copper-Catalyzed or Copper-Free Strain-Promoted Click Chemistry. *Nucleic Acids Res.* **2012**, *40*, e78.
36. Kuzmin, A.; Poloukhtine, A.; Wolfert, M. A.; Popik, V. V. Surface Functionalization Using Catalyst-Free Azide-Alkyne Cycloaddition. *Bioconjugate Chem.* **2010**, *21*, 2076–2085.
37. Hui, J. Z.; Al Zaki, A.; Cheng, Z.; Popik, V.; Zhang, H.; Luning Prak, E. T.; Tsourkas, A. Facile Method for the Site-Specific, Covalent Attachment of Full-Length IgG onto Nanoparticles. *Small* **2014**, *10*, 3354–3363.
38. Kotagiri, N.; Li, Z.; Xu, X.; Mondal, S.; Nehorai, A.; Achilefu, S. Antibody Quantum Dot Conjugates Developed *via* Copper-Free Click Chemistry for Rapid Analysis of Biological Samples Using a Microfluidic Microsphere Array System. *Bioconjugate Chem.* **2014**, *25*, 1272–1281.
39. Prim, D.; Rebeaud, F.; Cosandey, V.; Marti, R.; Passeraub, P.; Pfeifer, M. E. ADIBO-Based "Click" Chemistry for Diagnostic Peptide Micro-Array Fabrication: Physicochemical and Assay Characteristics. *Molecules* **2013**, *18*, 9833–9849.
40. Koo, H.; Lee, S.; Na, J. H.; Kim, S. H.; Hahn, S. K.; Choi, K.; Kwon, I. C.; Jeong, S. Y.; Kim, K. Bioorthogonal Copper-Free Click Chemistry *in Vivo* for Tumor-Targeted Delivery of Nanoparticles. *Angew. Chem., Int. Ed.* **2012**, *51*, 11836–11840.
41. Gounaris, A. D.; Perlmann, G. E. Succinylation of Pepsinogen. *J. Biol. Chem.* **1967**, *242*, 2739–2745.
42. Hermanson, G. T. *Bopconjugate Techniques*, 2nd ed.; Elsevier: Amsterdam, 2008.
43. Grimsley, G. R.; Scholtz, J. M.; Pace, C. N. A Summary of the Measured pK Values of the Ionizable Groups in Folded Proteins. *Protein Sci.* **2009**, *18*, 247–251.
44. Mentinova, M.; Barefoot, N. Z.; McLuckey, S. A. Solution *versus* Gas-Phase Modification of Peptide Cations with

NHS-Ester Reagents. *J. Am. Soc. Mass Spectrom.* **2012**, *23*, 282–289.
45. Krishnakumar, P.; Gyarfas, B.; Song, W.; Sen, S.; Zhang, P.; Krstic, P.; Lindsay, S. Slowing DNA Translocation through a Nanopore Using a Functionalized Electrode. *ACS Nano* **2013**, *7*, 10319–10326.
46. Wanunu, M. Nanopores: A Journey towards DNA Sequencing. *Phys. Life Rev.* **2012**, *9*, 125–158.
47. Stefureac, R.; Long, Y.-t.; Kraatz, H.-B.; Howard, P.; Lee, J. S. Transport of α-Helical Peptides through α-Hemolysin and Aerolysin Pores. *Biochemistry* **2006**, *45*, 9172–9179.
48. Meng, H.; Detillieux, D.; Baran, C.; Krasniqi, B.; Christensen, C.; Madampage, C.; Stefureac, R. I.; Lee, J. S. Nanopore Analysis of Tethered Peptides. *J. Pept. Sci.* **2010**, *16*, 701–708.
49. Christensen, C.; Baran, C.; Krasniqi, B.; Stefureac, R. I.; Nokhrin, S.; Lee, J. S. Effect of Charge, Topology and Orientation of the Electric Field on the Interaction of Peptides with the α-Hemolysin pore. *J. Pept. Sci.* **2011**, *17*, 726–734.
50. Carson, S.; Wilson, J.; Aksimentiev, A.; Wanunu, M. Smooth DNA Transport through a Narrowed Pore Geometry. *Biophys. J.* **2014**, *107*, 2381–2393.
51. Mathe, J.; Aksimentiev, A.; Nelson, D. R.; Schulten, K.; Meller, A. Orientation Discrimination of Single-Stranded DNA Inside the Alpha-Hemolysin Membrane Channel. *Proc. Natl. Acad. Sci. U. S. A.* **2005**, *102*, 12377–12382.
52. Muzard, J.; Martinho, M.; Mathe, J.; Bockelmann, U.; Viasnoff, V. DNA Translocation and Unzipping Through a Nanopore: Some Geometrical Effects. *Biophys. J.* **2010**, *98*, 2170–2178.
53. Ying, Y.-L.; Li, D.-W.; Liu, Y.; Dey, S. K.; Kraatz, H.-B.; Long, Y.-T. Recognizing the Translocation Signals of Individual Peptide-Oligonucleotide Conjugates Using an α-Hemolysin Nanopore. *Chem. Commun.* **2012**, *48*, 8784–8786.
54. Grajkowski, A.; Iak, J. C.; Gapeev, A.; Schindler, C.; Beaucage, S. L. Convenient Synthesis of a Propargylated Cyclic (3′-5′) Diguanylic Acid and Its "Click" Conjugation to a Biotinylated Azide. *Bioconjugate Chem.* **2010**, *21*, 2147–2152.
55. Kyte, J.; Doolittle, R. F. a Simple Method for Displaying the Hydropathic Character of a Protein. *J. Mol. Biol.* **1982**, *157*, 105–132.
56. Hosoya, O.; Chono, S.; Saso, Y.; Juni, K.; Morimoto, K.; Seki, T. Determination of Diffusion Coefficients of Peptides and Prediction of Permeability through a Porous Membrane. *J. Pharm. Pharmacol.* **2004**, *56*, 1501–1508.